

Order of Magnitude Smaller Limit on the Electric Dipole Moment of the Electron

The ACME Collaboration: J. Baron¹, W. C. Campbell², D. DeMille³, J. M. Doyle¹, G. Gabrielse¹, Y. V. Gurevich^{1,*}, P. W. Hess¹, N. R. Hutzler¹, E. Kirilov^{3,#}, I. Kozyryev^{3,†}, B. R. O’Leary³, C. D. Panda¹, E. S. Petrik¹, B. Spaun¹, A. C. Vutha⁴, A. D. West³

Abstract:

The Standard Model (SM) of particle physics is known to be incomplete. It fails to explain dark matter, and why matter survived annihilation with antimatter following the Big Bang. Proposed extensions to the SM, such as weak-scale Supersymmetry (SUSY), may explain these phenomena by positing the existence of new particles and new interactions that are not symmetric under the time-reversal (T) transformation. These same theories nearly always predict a small, yet potentially measurable, asymmetric charge distribution directed along the spin (\vec{S}) of the electron, an electric dipole moment (EDM, $\vec{d}_e = d_e \vec{S}/(\hbar/2)$), which is also asymmetric under T. The predicted value of d_e in these SM extensions is typically in the range of 10^{-27} – 10^{-30} e cm, orders of magnitude larger than is predicted by the SM. Here, we report a new search for the electron EDM using the polar molecule thorium monoxide (ThO). Our result, $d_e = (-2.1 \pm 3.7_{\text{stat}} \pm 2.5_{\text{syst}}) \times 10^{-29}$ e cm, corresponds to an upper limit of $|d_e| < 8.7 \times 10^{-29}$ e cm with 90 percent confidence, an order of magnitude improvement in sensitivity compared to the previous best limit¹. Our result sets strong constraints on new physics (SM extensions) associated with T-violating interactions at the TeV energy scale.

The exceptionally high internal effective electric field (\mathcal{E}_{eff}) of heavy neutral atoms and molecules can be used to precisely probe for d_e via the energy shift $U = -\vec{d}_e \cdot \vec{\mathcal{E}}_{\text{eff}}$. Valence electrons in the molecule travel relativistically when near the heavy nucleus, making \mathcal{E}_{eff} up to 10^6 times larger than any static laboratory field^{2,3}. The previous best limits on d_e have come from experiments with thallium (Tl) atoms⁴ ($|d_e| < 1.6 \times 10^{-27}$ e cm), and ytterbium fluoride (YbF) molecules^{1,5} ($|d_e| < 1.06 \times 10^{-27}$ e cm). Molecules have advantages over atoms as probes of d_e . They can be fully polarized in laboratory-scale electric fields, leading to values of \mathcal{E}_{eff} much greater than in atoms. The motional electric fields and geometric phases that ultimately limited the Tl measurement are suppressed, as demonstrated by the YbF experiment¹ (certain atoms offer a similar suppression⁶). The $^3\Delta_1$ electronic state used in ThO provides several additional advantages over other systems used to search for d_e . \mathcal{E}_{eff} can be reversed without reversing the laboratory field, simply by tuning a laser, aiding systematic error suppression, as first demonstrated using a similar state in lead oxide (PbO)^{7,8}. A new advantage of ThO is its near-vanishing magnetic moment, which reduces sensitivity to spurious magnetic fields^{9,10}. When fully polarized, as in this experiment, \mathcal{E}_{eff} for ThO is 6 and 1200 times larger than that attained in the YbF and Tl experiments, respectively, enhancing the intrinsic sensitivity to d_e .

To measure the electron EDM we perform a spin precession measurement^{9,11,12} on a molecular beam of $^{232}\text{Th}^{16}\text{O}$. A pulse of ThO molecules from a cryogenic buffer gas beam source^{13,14} (see Methods) passes between parallel electric field plates that generate a laboratory field $\mathcal{E}\hat{z}$ (Figure 1). Coherent superpositions of two ThO spin states, corresponding to a spin aligned in the xy plane, are prepared using optical pumping and state preparation lasers. Parallel electric ($\vec{\mathcal{E}}$) and magnetic ($\vec{\mathcal{B}}$) fields interact with the electric and magnetic dipole moments, causing torques and resulting in energy shifts. The sign of each shift depends on the relative orientation of the spin with respect to $\vec{\mathcal{E}}_{\text{eff}}$ and $\vec{\mathcal{B}}$, respectively. These shifts cause the two states to accumulate a relative phase as they travel through the parallel fields. This phase is equivalent to the angle by which the spin vector precesses in the xy plane; it is measured with a readout laser and fluorescence detection. d_e is proportional to the difference in phases between measurements with $\vec{\mathcal{E}}_{\text{eff}}$ reversed (by reversing $\vec{\mathcal{E}}$ or by using a laser to change the direction of $\vec{\mathcal{E}}_{\text{eff}}$ relative to $\vec{\mathcal{E}}$)^{15,16}.

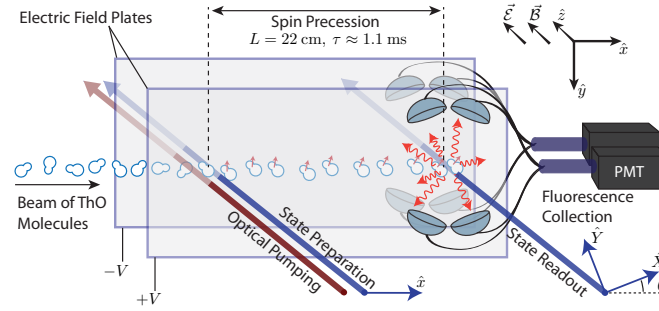


Figure 1: Schematic of the apparatus. A collimated pulse of ThO molecules enters a magnetically shielded region. An aligned spin state, prepared via optical pumping, precesses in applied electric and magnetic fields. The final spin alignment is read out by a laser with rapidly alternating linear polarizations, \hat{X}, \hat{Y} , with the resulting fluorescence collected and detected with photomultiplier tubes (PMTs).

In more detail, molecules pass through a 943 nm laser beam that optically pumps them from the ground electronic state into the ground rotational level, $J = 1$, of the metastable (lifetime ~ 2 ms) electronic $H^3\Delta_1$ state manifold, in an incoherent mixture of the

¹Department of Physics, Harvard University, 17 Oxford Street, Cambridge, Massachusetts 02138, USA. ²Department of Physics and Astronomy, University of California Los Angeles, 475 Portola Plaza, Los Angeles, CA 90095, USA. ³Department of Physics, Yale University, 217 Prospect Street, New Haven, Connecticut 06511, USA. ⁴Department of Physics and Astronomy, York University, 4700 Keele Street, Toronto, Ontario M3J 1P3, Canada. *Now at Department of Physics, Yale University, # Now at Institut für Experimentalphysik, Universität Innsbruck, Technikerstrasse 25/4, A-6020 Innsbruck, Austria. †Now at Department of Physics, Harvard University

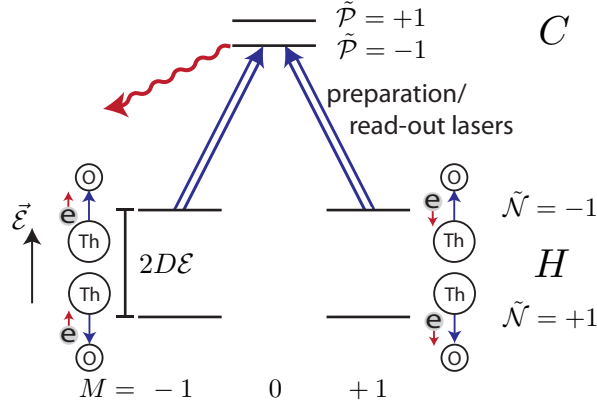


Figure 2: Energy level diagram showing the relevant states. The state-preparation and read-out lasers (double lined blue arrows) drive one molecule orientation $\tilde{N} = \pm 1$ (split by $2D\mathcal{E} \sim 100$ MHz) in the H state to C , with parity $\tilde{P} = \pm 1$ (split by 50 MHz). Population in the C state decays via spontaneous emission, and we detect the resulting fluorescence. H state levels are accompanied by cartoons displaying the orientation of the effective electric field (blue arrows) and the spin of the electron (red arrows) that dominantly contributes to the d_e shift.

$\tilde{N} = \pm 1$, $M = \pm 1$ states. M is the angular momentum projection along the \hat{z} axis. \tilde{N} refers to the induced molecular dipole moment, $D\hat{n}$, aligned (+1) or anti-aligned (-1) with respect to $\vec{\mathcal{E}}$, when $\mathcal{E} \gtrsim 1$ V/cm¹⁰. The molecules then enter a linearly polarized state-preparation laser beam, whose frequency is set on resonance with the $H \rightarrow C$ at 1090 nm (Figure 2). The C state is a short-lived (~ 500 ns) electronic state within which there are two opposite parity $\tilde{P} = \pm 1$ states with $J = 1, M = 0$. The laser frequency determines the \tilde{N}, \tilde{P} states that are addressed for a given spin precession measurement. This laser optically pumps the “bright” superposition of the two resonant $M = \pm 1$ sublevels out of the H state, leaving behind the “dark” orthogonal superposition. If the state-preparation laser is polarized along the \hat{x} axis, the prepared state, $|\psi(\hat{x}, \tau = 0), \tilde{N}\rangle$, has the electron spin aligned along the \hat{y} axis. The spin then precesses in the xy plane by angle ϕ to

$$|\psi(\hat{x}, \tau), \tilde{N}\rangle = (e^{-i\phi}|M = +1, \tilde{N}\rangle + e^{+i\phi}|M = -1, \tilde{N}\rangle)/\sqrt{2}. \quad (1)$$

Assuming $\vec{\mathcal{E}}$ and $\vec{\mathcal{B}}$ are aligned along \hat{z} , the phase ϕ is determined by $|\mathcal{B}_z| = |\vec{\mathcal{B}} \cdot \hat{z}|$, its sign, $\tilde{\mathcal{B}} = \text{sgn}(\vec{\mathcal{B}} \cdot \hat{z})$, and the electron’s EDM, d_e :

$$\phi \approx -(\mu_B g \tilde{\mathcal{B}} |\mathcal{B}_z| + \tilde{N} \tilde{\mathcal{E}} d_e \mathcal{E}_{\text{eff}}) \tau / \hbar, \quad (2)$$

where $\tilde{\mathcal{E}} \equiv \text{sgn}(\vec{\mathcal{E}} \cdot \hat{z})$, $\mu_B g$ is the magnetic moment¹² and τ is the spin precession time. The sign of the EDM term, $\tilde{N} \tilde{\mathcal{E}}$, is derived from the relative orientation between the internal electric field and the electron spin projection, as illustrated in Figure 2.

After the molecules precess over a distance of $L \approx 22$ cm (corresponding to $\tau \approx 1.1$ ms), we measure ϕ by optically pumping on the same $H \rightarrow C$ transition with the state readout laser. The laser polarization rapidly alternates between \hat{X} and \hat{Y} , and we record the fluorescence from the decay of C to the ground state (see Methods). This procedure amounts to projective measurements of the molecule alignment onto \hat{X} and \hat{Y} , which are defined such that \hat{X} is at an angle θ with respect to \hat{x} in the xy plane. This polarization switching results in modulated fluorescence signals S_X and S_Y , which result from the decay of molecules excited by the \hat{X} and \hat{Y} laser polarizations, respectively. To normalize our measurement to molecule number fluctuations, we compute the asymmetry,⁹

$$\mathcal{A} \equiv \frac{S_X - S_Y}{S_X + S_Y} = \mathcal{C} \cos(2(\phi - \theta)) \quad (3)$$

where \mathcal{C} is the contrast, a number that encodes our sensitivity to phase. We set $|\mathcal{B}_z|$ and θ such that $\phi - \theta \approx \frac{\pi}{4}(2n + 1)$ for integer n , so that the asymmetry is linearly proportional to small changes in ϕ , and maximally sensitive to the EDM. We measure the contrast, $|\mathcal{C}| = 94 \pm 2\%$, by dithering θ between two nearby values that differ by 0.1 rad, denoted by $\hat{\theta} = \pm 1$. This procedure allows us to extract a measurement of ϕ .

We perform this spin precession measurement repeatedly under varying experimental conditions in order to (a) distinguish the EDM energy shift from background phases and (b) search for and monitor possible systematic errors. Within a “block” of data taken over 40 s, we perform 4 identical measurements of the phase for each of a complete set of 2^4 experimental states derived from 4 binary switches, listed from fastest (.5 s) to slowest (20 s): the molecule alignment, \tilde{N} ; the direction of the applied electric field, $\tilde{\mathcal{E}}$; the readout laser polarization dither state, $\hat{\theta}$; and the magnetic field direction, $\tilde{\mathcal{B}}$. These reversals are important for the measurement because the EDM energy shift is odd under the \tilde{N} and $\tilde{\mathcal{E}}$ switches, the $\hat{\theta}$ switch is required to measure \mathcal{C} , and the $\tilde{\mathcal{B}}$ switch is required to measure τ . For each $(\tilde{N}, \tilde{\mathcal{E}}, \tilde{\mathcal{B}})$ state of the experiment, we measure \mathcal{A} and \mathcal{C} , from which we can extract ϕ . For data from each block, we form “parity components” of the phase, ϕ^p , which are combinations of the measured phases that are odd or even under these switch operations^{8,17}. We denote the experimental parity of a quantity with a superscript, listing the switch labels under which the quantity is odd; it is even under all unlabeled switches. These “parity components” correspond to particular physical effects that contribute to ϕ . For example, the EDM contributes a phase component $\phi^{\tilde{N}\tilde{\mathcal{E}}}$, which is odd under the \tilde{N} and $\tilde{\mathcal{E}}$ switches and even under the $\tilde{\mathcal{B}}$ switch, and we extract the mean precession time τ from the component of phase that is odd under only the $\tilde{\mathcal{B}}$ switch, $\phi^{\tilde{\mathcal{B}}} = -\mu_B g |\mathcal{B}_z| \tau / \hbar$. We then compute the frequency, $\omega^p \equiv \phi^p / \tau$, and extract the EDM measurement from $d_e = -\hbar \omega^{\tilde{N}\tilde{\mathcal{E}}} / \mathcal{E}_{\text{eff}}$.

On a slower time scale, from block to block, we perform additional “superblock” binary switches that are useful in the suppression of some known systematic errors and in the search for unknown ones. These switches, which occur on the 40–1200 s time scales, are: (1) the excited state parity addressed by the state read-out lasers, $\tilde{\mathcal{P}}$; (2) a rotation of the read-out polarization basis by $\theta \rightarrow \theta + \pi/2$, $\tilde{\mathcal{R}}$; (3) a reversal of the leads that supply the electric fields, $\tilde{\mathcal{L}}$; and (4) a global polarization rotation of both the state preparation and read-out laser polarizations, $\tilde{\mathcal{G}}$. Both the $\tilde{\mathcal{P}}$ and $\tilde{\mathcal{R}}$ switches interchange the role of the \hat{X} and \hat{Y} readout polarization beams and hence reject systematic errors associated with small differences in power, shape, or pointing between them. The two $\tilde{\mathcal{G}}$ state angles are chosen to suppress systematics that couple to unwanted ellipticity imprinted on the polarizations by a birefringence in the electric field plates. The $\tilde{\mathcal{L}}$ switch rejects systematics that couple to an offset voltage in the electric field power supplies. We define a complete “EDM measurement” as a set of the 2^8 block and superblock states. All of our systematic checks were performed with this experimental protocol. The extracted EDM value is even under all of the superblock switches.

The total dataset consists of about 10^4 blocks of data, taken over the course of ~ 2 weeks. During this dataset, in addition to the 8 switches described above, we also varied, from fastest (hours) to slowest (a few days): the \mathcal{B} -field magnitude, $|\mathcal{B}_z| \approx 1, 20, 40$ mG (corresponding to $|\phi| \approx 0, \pi/4, \pi/2$ respectively), the \mathcal{E} -field magnitude $|\mathcal{E}_z| \approx 36, 142$ V/cm, and the pointing direction of the lasers, $\hat{k} \cdot \hat{z} = \pm 1$. Previous EDM experiments were unable to operate at multiple electric fields due to incomplete atomic/molecular polarization. Figure 3b shows measured EDM values obtained when the dataset is grouped according to the states of $|\mathcal{B}_z|$, $|\mathcal{E}_z|$, $\hat{k} \cdot \hat{z}$, and each superblock switch. All of these measurements are consistent with the measured mean within 2σ . We also performed periodic auxiliary measurements during this dataset to monitor the dominant systematic errors, described below.

We compute the standard error in the mean and use standard Gaussian error propagation to obtain the reported statistical uncertainty. The reported upper limit is computed using the Feldman-Cousins prescription¹⁸ applied to a folded normal distribution at 90% confidence. To prevent experimental bias, we performed a blind analysis by adding an unknown offset to the EDM measurement. The mean, statistical error, systematic shifts, and procedure for calculating the systematic error were determined before unblinding. Our statistical distribution is consistent with a Gaussian; Figure 3a shows a histogram of EDM measurements grouped by block and by time within the molecular beam pulse. When fit to a constant value, the reduced chi-squared is $\chi^2 = .996 \pm .006$. Despite the empirical Gaussianity of the data, the asymmetry, \mathcal{A} , obeys a ratio distribution, which has large non-Gaussian tails in the limit of low signal to noise¹⁹. We apply a photon count rate threshold cut to the data so that we only include data with a large signal-to-noise ratio, resulting in a statistical distribution that approximates a Gaussian. Based on the total number of detected photons that contribute to the measurement, we determine the statistical uncertainty is 1.15 times that from photo-electron shot noise in the PMTs¹².

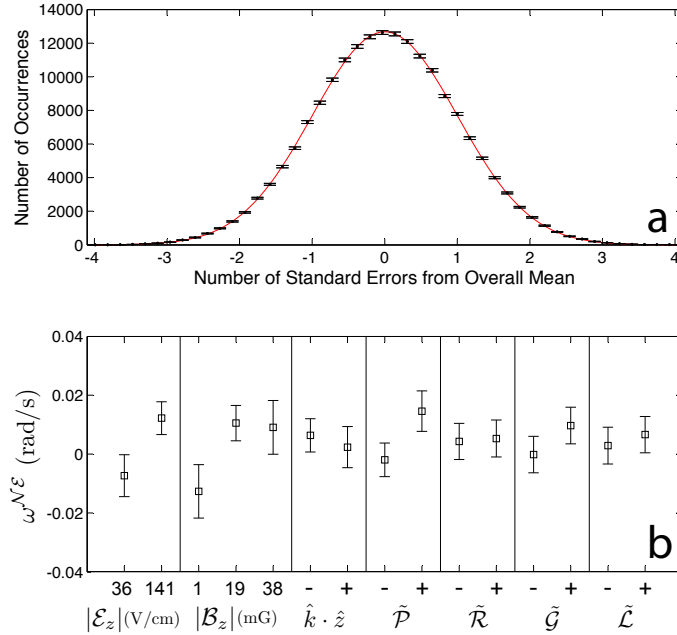


Figure 3: **a.** Histogram of $\omega^{\mathcal{N}\mathcal{E}}$ measurements for each time point (within molecule pulse) and for all blocks. Error bars represent expected Poissonian fluctuations in each histogram bin. **b.** Measured $\omega^{\mathcal{N}\mathcal{E}}$ values grouped by the states of $|\mathcal{B}_z|$, $|\mathcal{E}_z|$, $\hat{k} \cdot \hat{z}$, and each superblock switch, before systematic corrections.

To search for possible sources of systematic error, we tuned over 40 separate parameters and measured their effect on $\omega^{\mathcal{N}\mathcal{E}}$ and many other components of the phase correlated with $\hat{\mathcal{N}}$, $\hat{\mathcal{E}}$, or $\hat{\mathcal{B}}$. These parameters are intentionally applied tunable imperfections in the experiment, such as transverse magnetic fields or laser detunings.

Assuming that $\omega^{\mathcal{N}\mathcal{E}}$ depends linearly on each parameter P , the possible systematic shift and uncertainty of $\omega^{\mathcal{N}\mathcal{E}}$ is evaluated from the measured slope, $S = \partial\omega^{\mathcal{N}\mathcal{E}}/\partial P$, and the parameter value during normal operation (obtained from auxiliary measurements). If S was not monitored throughout the data set, we do not apply a systematic correction for that parameter but simply include an upper limit in our systematic error budget. Data taken with any parameter tuned outside of its nominal range was used only for determination

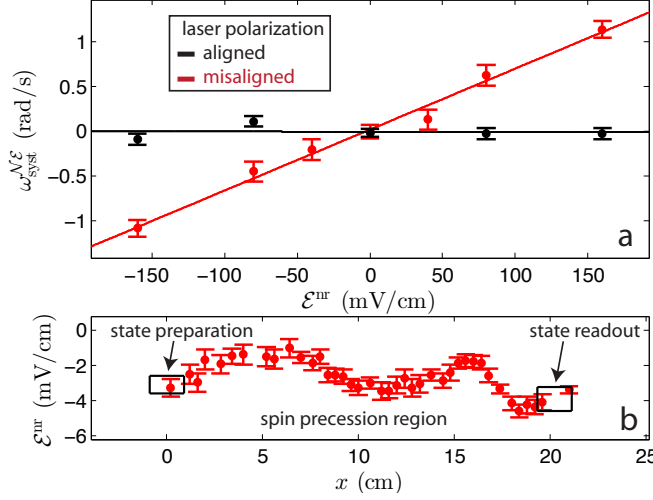


Figure 4: **a.** Tuning out laser polarization gradient and $\partial\omega^{\mathcal{N}\mathcal{E}}/\partial\mathcal{E}^{\text{nr}}$ (see text for details). The red (black) points were taken with the polarization misaligned (aligned) with the birefringence axes of the electric field plates. **b.** Microwave spectroscopic measurement of \mathcal{E}^{nr} along the molecule beam axis, x .

of systematic shifts and uncertainties. Table 1 contains a list of all contributions to our systematic error.

We discovered two parameters which systematically shift the value of $\omega^{\mathcal{N}\mathcal{E}}$ within our experimental resolution. Both couple to the AC Stark shift induced by the lasers. The molecules are initially prepared in the dark state with a spin orientation dependent on the laser polarization. If there is a polarization gradient along the molecular beam propagation direction, the molecules acquire a small bright state amplitude. Away from the center of a Gaussian laser profile, the laser can be weak enough that the bright state amplitude is not rapidly pumped away and it acquires a phase relative to the dark state due to their mutual energy splitting, given by the AC Stark shift. An equivalent phase is acquired in the state read-out laser. These phases depend on the detuning Δ relative to the $H \rightarrow C$ resonance and the Rabi frequency Ω_r (proportional to the electric field of the laser beam). This effect results in a change in the measured phase by an amount $\phi_{\text{AC}}(\Delta, \Omega_r) = \alpha\Delta + \beta\Omega_r$. The constants α and β are measured directly by varying the laser detuning and intensity, and depend on the laser's spatial intensity and polarization profile. These measurements are in good agreement with our analytic and numerical models.

A significant polarization gradient can be caused by laser-induced thermal stress birefringence²⁰ in the electric field plates. The lasers are elongated perpendicular to the molecular beam axis, which creates an asymmetric thermal gradient and defines the axes for the resulting birefringence gradient. By aligning the laser polarization with the birefringence axes, the polarization gradient can be minimized. We have verified this both with polarimetry²¹ and through the resulting AC Stark shift systematic (Figure 4a).

Such AC Stark shift effects can cause a systematic shift in our measurement of $\omega^{\mathcal{N}\mathcal{E}}$ if a detuning or Rabi frequency is correlated with $\tilde{\mathcal{N}}\tilde{\mathcal{E}}$. We observe both effects.

In addition to the ideally reversing component, $|\mathcal{E}_z|\tilde{\mathcal{E}}$, our electric field contains a non-reversing component \mathcal{E}^{nr} from patch potentials and technical voltage offsets. The \mathcal{E}^{nr} creates a correlated DC Stark shift and an associated detuning $\Delta^{\mathcal{N}\mathcal{E}} = D\mathcal{E}^{\text{nr}}$. We measured \mathcal{E}^{nr} via microwave spectroscopy (Figure 4b), two-photon Raman spectroscopy, and monitoring of the $\tilde{\mathcal{N}}\tilde{\mathcal{E}}$ -correlated contrast.

A component of the Rabi frequency correlated with $\tilde{\mathcal{N}}\tilde{\mathcal{E}}$, $\Omega_r^{\mathcal{N}\mathcal{E}}$, arises from a dependence of the Rabi frequency on the orientation of the molecular axis, $\hat{n} \approx \tilde{\mathcal{N}}\tilde{\mathcal{E}}\hat{z}$, with respect to laser propagation direction, \hat{k} . This $\hat{k} \cdot \hat{n}$ dependence can be caused by interference between E1 and M1 transition amplitudes on the $H \rightarrow C$ transition. Measurements of a non-zero $\tilde{\mathcal{N}}\tilde{\mathcal{E}}$ -correlated fluorescence signal and an $\tilde{\mathcal{N}}\tilde{\mathcal{E}}\tilde{\mathcal{B}}$ -correlated phase, both of which changed sign when we reversed \hat{k} , provided evidence for a nonzero $\Omega_r^{\mathcal{N}\mathcal{E}}$. These channels, along with their linear dependence on an artificial $\Omega_r^{\mathcal{N}\mathcal{E}}$ generated with an $\tilde{\mathcal{N}}\tilde{\mathcal{E}}$ correlated laser intensity, allowed us to measure $\Omega_r^{\mathcal{N}\mathcal{E}}/\Omega_r = (-8.0 \pm 0.8) \times 10^{-3}(\hat{k} \cdot \hat{z})$, where Ω_r is the uncorrelated (mean) Rabi frequency.

By intentionally exaggerating these parameters we verified that both \mathcal{E}^{nr} and $\Omega_r^{\mathcal{N}\mathcal{E}}$ could couple to AC Stark shift effects to produce a false EDM. Figure 4a illustrates our ability to suppress the measured $\omega^{\mathcal{N}\mathcal{E}}$ shift as a function of applied \mathcal{E}^{nr} . The correlations, $\partial\omega^{\mathcal{N}\mathcal{E}}/\partial\mathcal{E}^{\text{nr}}$ and $\partial\omega^{\mathcal{N}\mathcal{E}}/\partial\Omega_r^{\mathcal{N}\mathcal{E}}$, were monitored at regular intervals throughout the data set. The resulting systematic corrections to $\omega^{\mathcal{N}\mathcal{E}}$ were all < 1 mrad/s.

For a subset of our data, the $\tilde{\mathcal{N}}$ -correlated phase $\phi^{\mathcal{N}}$ was non-zero and drifted with time. We were able to identify the cause of this behavior as an $\tilde{\mathcal{N}}$ -correlated laser pointing $k^{\mathcal{N}} \approx 5 \mu\text{rad}$ present in our optical frequency switching setup. We were able to eliminate this effect with improved optical alignment; however, since we were not able to determine the precise mechanism by which $k^{\mathcal{N}}$ coupled to $\phi^{\mathcal{N}}$, we chose to include $\phi^{\mathcal{N}}$ variations in our systematic error budget. We fit a slope to a plot of $\omega^{\mathcal{N}\mathcal{E}}$ vs. $\phi^{\mathcal{N}}$ and then used the mean value of $\phi^{\mathcal{N}}$ to determine our systematic uncertainty, similar to the method used with intentionally varied parameters described earlier. The resulting slope was consistent with zero and allowed us to place a systematic uncertainty limit of ≈ 1 mrad/s on $\omega^{\mathcal{N}\mathcal{E}}$.

To be cautious, we also include in our systematic error budget possible contributions from effects associated with parameters that caused a non-zero $\omega^{\mathcal{N}\mathcal{E}}$ shift in experiments similar to ours, even if the effect should be suppressed in our experiment. Examples of

Parameter	Shift	Uncertainty
\mathcal{E}^{nr} correction	-0.81	0.66
$\Omega_{\text{r}}^{\mathcal{N}\mathcal{E}}$ correction	-0.03	1.58
$\phi^{\mathcal{E}}$ correlated effects	-0.01	0.01
$\phi^{\mathcal{N}}$ correlation		1.25
Non-Reversing \mathcal{B} -field ($\mathcal{B}_z^{\text{nr}}$)		0.86
Transverse \mathcal{B} -fields ($\mathcal{B}_x^{\text{nr}}, \mathcal{B}_y^{\text{nr}}$)		0.85
\mathcal{B} -Field Gradients		1.24
Prep./Read Laser Detunings		1.31
$\tilde{\mathcal{N}}$ Correlated Detuning		0.90
\mathcal{E} -field Ground Offset		0.16
Total Systematic	-0.84	3.24
Statistical		4.80
Total Uncertainty		5.79

Table 1: Systematic and statistical errors, in units of mrad/s. All errors are added in quadrature.

such parameters include stray magnetic fields $\mathcal{B}_{x,y,z}^{\text{nr}}$ and magnetic field gradients⁸; an $\tilde{\mathcal{E}}$ -correlated phase caused by leakage current, $\vec{v} \times \tilde{\mathcal{E}}$, and geometric phase effects⁴; and various laser detunings and \mathcal{E} -field ground offsets¹. By intentionally exaggerating each of these parameters, we obtained a direct $\omega^{\mathcal{N}\mathcal{E}}$ systematic limit of $\lesssim 1$ mrad/s for each parameter. We exaggerated the $\tilde{\mathcal{E}}$ -correlated phase $\phi^{\mathcal{E}}$ by intentionally correlating \mathcal{B}_z with $\tilde{\mathcal{E}}$, allowing us to place a $\sim 10^{-2}$ mrad/s limit on possible $\omega^{\mathcal{N}\mathcal{E}}$ shifts arising from leakage current, $\vec{v} \times \tilde{\mathcal{E}}$, and geometric phase effects. We emphasize that because of our slow molecular beam, our relatively small applied electric fields, and the small magnetic dipole moment of the H state, we do not expect any of these effects to systematically shift $\omega^{\mathcal{N}\mathcal{E}}$ above the 10^{-3} mrad/s level^{9,10}.

The result of this first-generation ThO measurement,

$$d_e = (-2.1 \pm 3.7_{\text{stat}} \pm 2.5_{\text{syst}}) \times 10^{-29} \text{ e cm}, \quad (4)$$

comes from $d_e = -\hbar\omega^{\mathcal{N}\mathcal{E}}/\mathcal{E}_{\text{eff}}$ using $\mathcal{E}_{\text{eff}} = 84 \text{ GV/cm}$ ^{15,22} and $\omega^{\mathcal{N}\mathcal{E}} = (2.6 \pm 4.8_{\text{stat}} \pm 3.2_{\text{syst}}) \text{ mrad/s}$. This sets a 90 percent confidence limit,

$$|d_e| < 8.7 \times 10^{-29} \text{ e cm}, \quad (5)$$

that is 12 times smaller than the previous best limit^{1,4}. Because paramagnetic molecules are sensitive to multiple T-violating effects²³, our measurement should be interpreted as $\hbar\omega^{\mathcal{N}\mathcal{E}} = -d_e\mathcal{E}_{\text{eff}} - W_S C_S$, where C_S is a T-violating electron-nucleon coupling, and W_S is a molecule-specific constant which has been calculated for ThO^{15,16}. In keeping with convention, we assume $C_S = 0$ for the limit written above. Assuming instead that $d_e = 0$ yields $C_S = (-1.3 \pm 3.0) \times 10^{-9}$, corresponding to a 90 percent confidence limit $|C_S| < 5.9 \times 10^{-9}$ that is 9 times smaller than the earlier limit²⁴.

A measurably large EDM requires new mechanisms for T violation (equivalent to charge-parity [CP] violation, assuming that the combined symmetry CPT is conserved²) beyond those in the SM. Nearly every extension to the SM includes such mechanisms. The effective strength of CP violation is proportional to the sine of a phase, ϕ_{CP} . It is difficult to construct mechanisms that systematically suppress such phases, so model builders typically assume $\sin(\phi_{\text{CP}}) \approx 1$ ²⁵. In this case, simple dimensional estimates can be made for d_e , which can be calculated from Feynman diagrams including loops that contain new particles or fields (where the number of loops corresponds to the order of perturbation theory at which they arise). An EDM arising from new CP-violating phenomena at energy Λ in an n -loop diagram will have size $d_e/e \sim \kappa(\alpha_{\text{eff}}/4\pi)^n(m_e c^2/\Lambda^2)(\hbar c)^{-1}$, where α_{eff} encodes the strength with which the electron couples to the new phenomena, m_e is the electron mass, and κ is a dimensionless constant of order 1^{2,26,27}. An upper bound to the scale of new physics $\Lambda \approx 30 \text{ TeV}$ probed by the EDM arises when $\alpha_{\text{eff}} = 1$ and $n = 1$. In certain supersymmetric models (where strong mixing between particle families is allowed), our result probes this energy scale²⁷. In many models, $\alpha_{\text{eff}} \sim 4/137$ (the coupling strength of electroweak interactions) and typically $\kappa \sim 0.2$ ²⁸. Then, in models where 1- or 2-loop diagrams produce the EDM, our result sets a bound on CP-violation at energy scales $\Lambda \sim 3 \text{ TeV}$ or 1 TeV , respectively. Predictions for the electron EDM in both of these cases have been calculated in the context of many models^{29,30}. Though details differ, these estimates are typical of the results. Notably, in almost every case our experiment is predicted to probe energy scales similar to or higher than those explored directly at the Large Hadron Collider (LHC). Our result is also complementary to the LHC, since it is a direct test for new sources of CP violation.

Our measurement has improved the electron EDM limit by a factor of 12 by the first use of the ThO molecule and of a cryogenic source of cold molecules for this purpose. ThO has an enormous effective internal field that is easily aligned and saturated with a small laboratory field, and can be reversed spectroscopically with no change in laboratory field. Simple arguments show that the energy being probed is comparable to or higher than what is currently being investigated by the LHC. A reduction in uncertainty in a next-generation experiment will either discover the long-predicted electron EDM or further constrain proposed extensions to the Standard Model and their CP-violating interactions.

Methods

We create a pulsed molecular beam of ThO using the buffer gas beam technique^{31,14,13}. Each packet of molecules leaving the source contains $\sim 10^{11}$ ThO molecules in the $J = 1$ rotational level of the ground electronic (X) and vibrational states and are produced at a

repetition rate of 50 Hz. The packet is 2-3 ms wide and has a center of mass speed of ~ 200 m/s. After leaving the cryogenic beam source chamber, the molecules travel through a microwave field resonant with the $|X; J = 1\rangle \leftrightarrow |X; J = 0\rangle$ transition and optical pumping lasers resonant with the $|X; J = 2, 3\rangle \rightarrow |C; J = 1, 2\rangle$ transitions. The microwaves and optical pumping lasers transfer population from $|X; J = 0, 2, 3\rangle$ into the $|X; J = 1\rangle$ state leading to a twofold increase in its population. The molecules then pass through adjustable and fixed collimating apertures before entering the magnetically shielded interaction region, where electric and magnetic fields are applied. A retroreflected 943 nm laser optically pumps population from the $|X; J = 1, M = \pm 1\rangle$ states to $|A; J = 0, M = 0\rangle$, which decays partially into the $|H; J = 1\rangle$ state in which the EDM measurement is performed.

The spin precession region contains applied electric and magnetic fields, along with lasers to prepare and read our EDM state. The electric field is provided by two plates of 12.7 mm thick glass coated with a layer of indium tin oxide (ITO) on one side, and an anti-reflection coating on the other. The ITO coated sides of the plates face each other with a gap of 25 mm, and a voltage is applied to the ITO to create a uniform electric field.

The spatial profile of the electric field was measured by performing microwave spectroscopy on the ThO molecules. When the molecule pulse is between the state preparation and read-out regions, a 40 μ s burst of microwaves resonant with the DC Stark-shifted $|H; J = 1, M = \pm 1\rangle \rightarrow |H; J = 2, M = 0\rangle$ transitions is introduced by a microwave horn at the end of the apparatus, counterpropagating to the molecular beam. If on resonance the microwaves drive a transition that spin-polarizes the molecules, similar to the state preparation scheme. We can then detect the spin polarization using the normal readout scheme. The microwave transition width is ~ 5 kHz (dominated by Doppler broadening), so the H -state dipole moment of $D \approx 1$ MHz/(V/cm)¹⁰ (for $J = 1$) means that this method is sensitive to \sim mV/cm electric field deviations with spatial resolution of ≈ 1 cm, limited by the velocity distribution in the beam. Our measurement indicated that the spatial variation of the electric field plate separation is ~ 20 μ m across the molecule precession region, in very good agreement with an interferometric measurement³². We can also test how well the electric field reverses by mapping the field with equal and opposite voltages on the plates. This measurement indicated that the non-reversing component of the electric field had magnitude $|\mathcal{E}^{\text{nr}}| \approx 1$ -5 mV/cm across the entire molecular precession region, as shown in Figure 4b.

The EDM measurement is performed in a vacuum chamber surrounded by five layers of mu-metal shielding. The applied magnetic field is supplied by a cosine-theta coil, with several shim coils to create a more uniform magnetic field within the precession region, and to allow us to apply transverse magnetic fields and gradients for systematic checks. Changes in the magnetic field are monitored by four 3-axis fluxgate magnetometers inside the magnetic shields, and the magnetic fields were mapped out before and after the experimental dataset was taken by sliding a 3-axis fluxgate down the beamline.

The lasers travel through the electric field plates, so all stages of the spin precession measurement are performed inside the uniform electric field. All laser light in the experiment originates from external cavity diode lasers (ECDL), frequency stabilized via an Invar transfer cavity to a CW Nd:YAG laser locked to a molecular iodine transition³³. All required transition frequencies and state assignments were determined previously^{34,35,36}. We measured the saturation intensities, radiative lifetimes, electric/magnetic dipole moments, and branching ratios for all required states and transitions.

In order to normalize against drifting molecular beam properties (pulse shape, total molecule number, velocity mean and distribution, etc.), we perform a spin precession measurement every 10 μ s, which is much faster than the molecular beam variations¹², spin precession time and temporal width of the molecular pulse. This is accomplished by sending the detection laser through two different beam paths, combined on the two ports of a polarizing beamsplitter. The two beam paths can be rapidly switched on and off with acousto-optic modulators.

The transparent electric field plates allow us to collect a large fraction of the solid angle of fluorescence from the molecules. Fluorescence travels through the field plates into an eight-lens system (four behind each plate) which focuses the light into an optical fiber bundle. The four bundles on each side are coupled into a fused quartz light pipe, which carries the fluorescence to a PMT (outside the magnetic shields). The net detection efficiency, including collection solid angle and detector quantum efficiency, is $\approx 1\%$. We typically register ≈ 1000 photon counts per molecule pulse. The PMT photocurrents are read as analog signals by a low-noise, high-bandwidth amplifier, and then sent to a 24-bit digitizer operating at 5 megasamples/s. The control and timing for all experimental parameters is managed by a single computer, and the timing jitter is less than one digitizer sampling period.

References

1. J. J. Hudson, D. M. Kara, I. J. Smallman, B. E. Sauer, M. R. Tarbutt, and E. A. Hinds, "Improved measurement of the shape of the electron," *Nature*, vol. 473, pp. 493–6, May 2011.
2. I. B. Khriplovich and S. K. Lamoreaux, *CP Violation Without Strangeness*. Springer, 1997.
3. P. G. H. Sandars, "The Electric Dipole Moment of an Atom," *Physics Letters*, vol. 14, p. 194, Feb. 1965.
4. B. Regan, E. Commins, C. Schmidt, and D. DeMille, "New Limit on the Electron Electric Dipole Moment," *Physical Review Letters*, vol. 88, pp. 18–21, Feb. 2002.
5. D. M. Kara, I. J. Smallman, J. J. Hudson, B. E. Sauer, M. R. Tarbutt, and E. A. Hinds, "Measurement of the electron's electric dipole moment using YbF molecules: methods and data analysis," *New Journal of Physics*, vol. 14, p. 103051, Oct. 2012.
6. M. A. Player and P. G. H. Sandars, "An experiment to search for an electric dipole moment in the 3P_2 metastable state of xenon," *J. Phys. B*, vol. 3, pp. 1620–1635, 1970.

7. S. Bickman, P. Hamilton, Y. Jiang, and D. DeMille, "Preparation and detection of states with simultaneous spin alignment and selectable molecular orientation in PbO," *Physical Review A*, vol. 80, p. 023418, Aug. 2009.
8. S. Eckel, P. Hamilton, E. Kirilov, H. W. Smith, and D. DeMille, "Search for the electron electric dipole moment using Ω -doublet levels in PbO," *Physical Review A*, vol. 87, p. 052130, May 2013.
9. A. C. Vutha, W. C. Campbell, Y. V. Gurevich, N. R. Hutzler, M. Parsons, D. Patterson, E. Petrik, B. Spaun, J. M. Doyle, G. Gabrielse, and D. DeMille, "Search for the electric dipole moment of the electron with thorium monoxide," *Journal of Physics B*, vol. 43, p. 74007, Apr. 2010.
10. A. C. Vutha, B. Spaun, Y. V. Gurevich, N. R. Hutzler, E. Kirilov, J. M. Doyle, G. Gabrielse, and D. DeMille, "Magnetic and electric dipole moments of the $H^3\Delta_1$ state in ThO," *Physical Review A*, vol. 84, p. 034502, Sept. 2011.
11. W. C. Campbell, C. Chan, D. Demille, J. M. Doyle, G. Gabrielse, Y. V. Gurevich, P. W. Hess, N. R. Hutzler, E. Kirilov, B. O. Leary, E. S. Petrik, B. Spaun, and A. C. Vutha, "Advanced cold molecule electron EDM," *EPJ Web of Conferences*, vol. 57, p. 02004, Aug. 2013.
12. E. Kirilov, W. C. Campbell, J. M. Doyle, G. Gabrielse, Y. V. Gurevich, P. W. Hess, N. R. Hutzler, B. R. OLeary, E. Petrik, B. Spaun, A. C. Vutha, and D. DeMille, "Shot-noise-limited spin measurements in a pulsed molecular beam," *Physical Review A*, vol. 88, p. 013844, July 2013.
13. S. E. Maxwell, N. Brahms, R. DeCarvalho, D. R. Glenn, J. S. Helton, S. V. Nguyen, D. Patterson, J. Petricka, D. DeMille, and J. M. Doyle, "High-Flux Beam Source for Cold, Slow Atoms or Molecules," *Physical Review Letters*, vol. 95, p. 173201, Oct. 2005.
14. N. R. Hutzler, M. F. Parsons, Y. V. Gurevich, P. W. Hess, E. Petrik, B. Spaun, A. C. Vutha, D. DeMille, G. Gabrielse, and J. M. Doyle, "A cryogenic beam of refractory, chemically reactive molecules with expansion cooling," *Physical Chemistry Chemical Physics : PCCP*, vol. 13, pp. 18976–85, Nov. 2011.
15. L. V. Skripnikov, A. N. Petrov, and A. V. Titov, "Theoretical study of ThO for the electron electric dipole moment search," *arXiv:1308.0414*, Aug. 2013.
16. V. A. Dzuba, V. V. Flambaum, and C. Harabati, "Relations between matrix elements of different weak interactions and interpretation of the parity-nonconserving and electron electric-dipole-moment measurements in atoms and molecules," *Phys. Rev. A*, vol. 84, p. 052108, Nov 2011.
17. P. Hamilton, *Preliminary results in the search for the electron electric dipole moment in PbO*. PhD thesis, Yale University, 2010.
18. G. J. Feldman and R. D. Cousins, "Unified approach to the classical statistical analysis of small signals," *Physical Review D*, vol. 57, pp. 3873–3889, Apr. 1998.
19. J. H. Curtiss, "On the Distribution of the Quotient of Two Chance Variables," *The Annals of Mathematical Statistics*, vol. 12, pp. 409–421, Dec. 1941.
20. S. Eisenbach and H. Lotem, "Thermally induced window birefringence in high-power copper vapor laser," *SPIE 8th Meeting on Optical Engineering in Israel*, vol. 1972, 1992.
21. H. G. Berry, G. Gabrielse, and A. E. Livingston, "Measurement of the Stokes parameters of light," *Applied Optics*, vol. 16, pp. 3200–5, Dec. 1977.
22. E. R. Meyer and J. L. Bohn, "Prospects for an electron electric-dipole moment search in metastable ThO and ThF⁺," *Phys. Rev. A*, vol. 78, no. 1, p. 10502, 2008.
23. M. G. Kozlov and L. N. Labzowsky, "Parity violation effects in diatomics," *Journal of Physics B: Atomic, Molecular and Optical Physics*, vol. 28, pp. 1933–1961, May 1995.
24. W. Griffith, M. Swallows, T. Loftus, M. Romalis, B. Heckel, and E. Fortson, "Improved Limit on the Permanent Electric Dipole Moment of ¹⁹⁹Hg," *Physical Review Letters*, vol. 102, p. 101601, Mar. 2009.
25. J. Engel, M. J. Ramsey-Musolf, and U. van Kolck, "Electric dipole moments of nucleons, nuclei, and atoms: The Standard Model and beyond," *Progress in Particle and Nuclear Physics*, vol. 71, pp. 21–74, July 2013.
26. N. Fortson, P. Sandars, and S. Barr, "The search for a permanent electric dipole moment," *Physics Today*, vol. 56, no. 6, pp. 33–39, 2003.
27. W. Altmannshofer, R. Harnik, and J. Zupan, "Low Energy Probes of PeV Scale Sfermions," *arXiv:1308.3653*, 2013.
28. W. Bernreuther and M. Suzuki, "The electric dipole moment of the electron," *Reviews of Modern Physics*, vol. 63, no. 2, p. 313, 1991.

29. S. Barr, “A Review of CP Violation in Atoms,” *International Journal of Modern Physics A*, vol. 08, pp. 209–236, Jan. 1993.
30. M. Pospelov and A. Ritz, “Electric dipole moments as probes of new physics,” *Ann. Phys.*, vol. 318, pp. 119–169, July 2005.
31. N. R. Hutzler, H.-I. Lu, and J. M. Doyle, “The buffer gas beam: an intense, cold, and slow source for atoms and molecules,” *Chemical Reviews*, vol. 112, pp. 4803–27, Sept. 2012.
32. R. A. Patten, “Michelson Interferometer as a Remote Gauge,” *Applied Optics*, vol. 10, no. 12, pp. 2717–2721, 1971.
33. J. Hall, L.-S. Ma, M. Taubman, B. Tiemann, F. Hong, O. Pfister, and J. Ye, “Stabilization and frequency measurement of the I_2 -stabilized Nd:YAG laser,” *IEEE Transactions On Instrumentation And Measurement*, vol. 48, no. 2, pp. 583–586, 1998.
34. G. Edvinsson, A. Bornstedt, and P. Nylén, “Rotational Analysis for a Perturbed $^1\Pi$ state in ThO,” *Ark. Phys.*, vol. 38, p. 193, 1968.
35. G. Edvinsson and A. Lagerqvist, “Two new band systems in ThO,” *Physica Scripta*, vol. 41, pp. 316–320, 1990.
36. J. Paulovic, T. Nakajima, K. Hirao, R. Lindh, and P. A. Malmqvist, “Relativistic and correlated calculations on the ground and excited states of ThO,” *J. Chem. Phys.*, vol. 119, no. 2, pp. 798–805, 2003.

Acknowledgements We gratefully acknowledge conversations with Matt Reece and Matt Schwartz. We also acknowledge support of the NIST Precision Measurement Grant program and the National Science Foundation for their support. We also acknowledge the assistance of Stan Cotreau, Jim MacArthur, and Steve Sansone in constructing the apparatus.

Author Information The authors declare no competing financial interests. Correspondence and requests for materials should be addressed to acme@cua.harvard.edu.